Article

Journal of
Nanoscience and Nanotechnology
Vol. 16, 6432–6439, 2016
www.aspbs.com/jnn

Synchrotron Small-Angle X-ray Scattering Study of Cross-Linked Polymeric Micelles

Hyun-Chul Kim[1,*], Kyeong Sik Jin[2,*], Se Guen Lee[1], Eunjoo Kim[1], Sung Jun Lee[1], Sang Won Jeong[1], Seung Woo Lee[3], and Kwang-Woo Kim[2]

[1] *Nano and Bio Research Division, Daegu Gyeongbuk Institute of Science and Technology (DGIST), Daegu 711-873, Korea*
[2] *Pohang Accelerator Laboratory, Pohang University of Science and Technology (POSTECH), Pohang 790-784, Korea*
[3] *School of Display and Chemical Engineering, Yeungnam University, Gyeongsan 712-749, Korea*

Polymeric micelles of methoxypoly(ethylene glycol)-*b*-poly(lactide) containing lysine units (mPEG-PLA-Lys_4) were cross-linked by reacting of lysine moieties with a bifunctional bis(*N*-hydroxy-succinimide ester). The micelles were characterized in aqueous solution using dynamic light scattering, transmission electron microscopy, and synchrotron small-angle X-ray scattering. The mPEG-PLA-Lys_4 was synthesized through the ring-opening polymerization of N^6-carbobenzyloxy-L-lysine *N*-carboxyanhydride with amine-terminated mPEG-PLA and subsequent deprotection. The polymeric micelles showed enhanced micelle stability after cross-linking, which was confirmed by adding sodium dodecyl sulfate as a destabilizing agent. The average diameters measured via dynamic light scattering were 19.1 nm and 29.2 nm for non-cross-linked polymeric micelles (NCPMs) and cross-linked polymeric micelles (CPMs), respectively. The transmission electron microscopy images showed that the size of the polymeric micelles increased slightly due to cross-linking, which was in good agreement with the DLS measurements. The overall structures and internal structural changes of NCPMs and CPMs in aqueous solution were studied in detail using synchrotron X-ray scattering method. According to the structural parameters of X-ray scattering analysis, CPMs with a more densely packed core structure were formed by reacting bifunctional cross-linking agents with lysine amino groups located in the innermost core of the polymeric micelles.

Keywords: Polymeric Micelles, Cross-Linking, Synchrotron Small-Angle X-ray Scattering.

1. INTRODUCTION

Amphiphilic block copolymers consisting of a hydrophilic headgroup and a hydrophobic core can be self-assembled into spherical micelles, micellar cylinders, and vesicles, with core–shell architectures in aqueous media.[1,2] In particular, polymeric micelles have attracted significant attention due to their potential use in drug delivery systems (DDS), such as hydrophobic drug solubilizations, controlled drug release, and drug targeting.[3,4] Due to the dynamic nature of polymeric micelles, they are easily destabilized at high temperatures, under physiological conditions and in the presence of specific changes in solvent conditions.[5–7] A well-known approach to overcome these drawbacks is micelle cross-linking, which may enhance its structural stability in solution and reduce the leakage of encapsulated drugs.[8–10]

Polymeric micelles and cross-linked micelles have been investigated by dynamic light scattering (DLS) and transmission electron microscopy (TEM).[11,12] However, many of these techniques have yielded a limited amount of information about the structure of the assembly as a whole and the overall hydrodynamic micelle size.[13–15] Small-angle neutron scattering (SANS) and small-angle X-ray scattering (SAXS) have been widely used to determine various structural parameters, such as the size, shape, and internal structures of nanometer-scale particles in solution.[16–27] Riley et al. performed a structural analysis on poly(ethylene glycol)-*b*-poly(lactic acid) (PEG-*b*-PLA) micelles using SANS and determined that the shell thickness and PEG block conformation were

*Authors to whom correspondence should be addressed.

 1533-4880/2016/16/6432/008 doi:10.1166/jnn.2016.12108

correlated with the PLA core size.[25] Using SANS, Bhattacharjee et al. showed that the core size of doxorubicin-loaded poly(ethylene oxide)-poly(propylene oxide)-poly(ethylene oxide) triblock copolymer did not change significantly upon drug loading.[26] Akiba et al. carried out a SAXS study of a polymeric micelle solution made of partially benzyl-esterified poly(ethylene glycol)-*b*-poly(aspartic acid) (PEG-P(Asp(Bzl)) and found that the scattering profiles showed characteristic features of core–shell spherical micelles. Furthermore, they confirmed that PEG and P (Asp(Bzl)) formed a hydrophilic shell and a hydrophobic core, respectively.[27] Although many microscopy studies on the morphology of polymeric micelles have been done by using tools such as cryo-TEM, SANS, and SAXS, to the best of our knowledge, there are no reports on SAXS study to determine the internal structures of the cross-linked polymeric micelles in solution.[16–27]

Herein, we describe the preparation of cross-linked polymeric micelles (CPMs) using an amphiphilic methoxypoly(ethylene glycol)-*b*-poly(DL-lactide)-(L-lysine) (mPEG-PLA-Lys_4) copolymer and an amine-reactive bifunctional bis(*N*-hydroxysuccinimide ester) containing a central disulfide bond. The morphological information related to size and shape of CPMs was compared to those of non-cross-linked polymeric micelles (NCPMs) using DLS and TEM. To obtain more detailed information on the structure in solution, we investigated the morphology, size, shape, and internal structures of NCPMs and CPMs through the fitting of scattering data obtained by SAXS. The cross-linked polymeric micelles used in this experiment are underway *in vitro* and *in vivo* tests to evaluate its potential as drug carrier.

2. EXPERIMENTAL DETAILS

2.1. Materials

Methoxypoly(ethylene glycol)-*b*-poly(lactide) (mPEG-PLA) with a molecular weight of 8000 (mPEG5000, PLA3000) was purchased from Advanced Polymer Material. Boc-aminohexanoic acid (Boc-Ahx-OH), dicyclohexylcarbodiimide (DCC), N^6-carbobenzyloxy-L-lysine, trichloromethyl chloroformate (TCF), thiohexanoic acid, and *N*-hydroxysuccinimide were obtained from Sigma-Aldrich and were used as received. Conventional chemicals employed in the present study were reagent grade and used as purchased without further purification.

2.2. Measurements

Nuclear magnetic resonance (NMR) spectra were obtained in $CDCl_3$ and DMSO using a Bruker NMR spectrometer (Aspect 3000 FT 400 MHz). The average size and zeta-potential of the polymeric micelles was measured via dynamic light scattering (DLS, Zetasizer Nano ZS, Malvern instrument). To observe the size and distribution of polymeric micelles, transmission electron microscopy (TEM) was performed on a Tecnai G2 (FEI company, USA) at an acceleration voltage of 120 kV. The samples were stained with uranyl acetate.

2.3. Synthesis of mPEG-PLA-Lys_4

mPEG-PLA-Ahx-Boc: mPEG-PLA (2.0 g, 0.25 mmol) was dissolved in anhydrous dichloromethane (50 mL), and Boc-6-Ahx-OH (0.12 g, 0.5 mmol) and DCC (0.1 g, 0.5 mmol) were added to the solution. The mixture was allowed to react for 48 h at room temperature, and dicyclohexylurea was removed by filtration. Excess acetone was added to the crude product mixture to precipitate residual dicyclohexylurea. After the precipitates were filtered out of solution, the solvent was removed by rotary evaporation. The product was precipitated from excess of cold diethyl ether. The polymer was collected and dried under vacuum to give mPEG-PDLLA-Ahx-Boc. Yield = 1.9 g. ^{1}H NMR δ (ppm): 5.18 (*m*, –C(O)CH(CH_3)O–), 3.63 (*m*, $CH_3OCH_2CH_2O$–), 3.40 (*s*, $CH_3OCH_2CH_2O$–), 1.70 (*d*, –C(O)$CH_2(CH_2)_2CH_2$NH–), 1.56 (*m*, –C(O)CH(CH_3)O–), 1.49 (*d*, –C(O)OC(CH_3)$_3$).

mPEG-PLA-NH_2: mPEG-PLA-Ahx-Boc (1.5 g) was dissolved in dichloromethane (10 mL) and the solution was cooled using an ice-bath. The reaction mixture was treated with trifluoroacetic acid (TFA, 5 mL) for 1 h. The solution was concentrated and the crude product was precipitated from cold diethyl ether. The polymer was collected and dried under vacuum at room temperature. Yield = 1.2 g. ^{1}H NMR δ (ppm): 5.18 (*m*, –C(O)CH(CH_3)O–), 3.63 (*m*, $CH_3OCH_2CH_2O$–), 3.40 (*s*, $CH_3OCH_2CH_2O$–), 1.70 (*d*, –C(O)$CH_2(CH_2)_2CH_2$NH–), 1.56 (*m*, –C(O)CH(CH_3)O–).

mPEG-PLA-Lys(Z)$_4$: In a dried flask, mPEG-PLA-NH_2 (1.0 g) and Lys(Z)-NCA (0.19 g, 0.62 mmol) were dissolved in a mixture of $CHCl_3$ (20 mL) and DMF (5 mL) under a nitrogen atmosphere. The reaction was allowed to proceed for 72 h at 35 °C. The mixture was precipitated with excess cold diethyl ether under stirring to give a white solid. The precipitate was dried under vacuum at 35 °C. Yield = 0.91 g. ^{1}H NMR δ (ppm): 7.33 (*s*, –C(O)OCH_2(C_6H_5)), 5.18 (*m*, –C(O)CH(CH_3)O–), 5.07 (*s*, –C(O)OCH_2(C_6H_5)) 3.63 (*m*, $CH_3OCH_2CH_2O$–), 3.40 (*s*, $CH_3OCH_2CH_2O$–), 3.10 (–C(O)CHNH–), 1.70 (*d*, –C(O)$CH_2(CH_2)_2CH_2$NH–), 1.56 (*m*, –C(O)CH(CH_3)O–), 1.25 (–(CH_2)$_4$NH–).

mPEG-PLA-Lys_4: In a dried flask, mPEG-PLA-Lys(Z)$_4$ (0.7 g) was dissolved in TFA (10 mL) and a solution of HBr (3 mL, 33 wt% in acetic acid) was added. The reaction mixture was stirred under nitrogen for 3 h at 0 °C. The solvent was removed under vacuum, and the crude product was precipitated with excess of diethyl ether to give a white solid. The resulting polymer was dried under vacuum at room temperature for 24 h to give PEG-PLA-Lys_4. Yield = 0.54 g. ^{1}H NMR δ (ppm): 7.71 (–C(O)CH_2NH–), 5.18 (*m*, –C(O)CH(CH_3)O–), 3.63 (*m*, $CH_3OCH_2CH_2O$–), 3.40 (*s*, $CH_3OCH_2CH_2O$–), 3.24 (–C(O)CHNH–), 1.70 (*d*, –C(O)$CH_2(CH_2)_2CH_2$NH–), 1.56 (*m*, –C(O)CH(CH_3)O–), 1.25 (–(CH_2)$_4$NH–).

2.4. Synthesis of N^6-Carbobenzyloxy-L-lysine N-carboxyanhydride (Lys(Z)-NCA) and bis(N-succinimido)-6,6-dithiobis (hexyl succinate)

N^6-Carbobenzyloxy-L-lysine (5.0 g, 17.8 mmol) and activated charcoal (0.3 g) were suspended in tetrahydrofuran (70 mL). TCF (3.5 mL, 25 mmol) was added to the suspension under vigorous stirring. The temperature was increased to 60 °C, and the reaction was continued until the N^6-carbobenzyloxy-L-lysine dissolved completely. The solution was filtered through Celite using a glass filter, and the filtrate was concentrated under vacuum to give a brown oil. The crude product was crystallized from ethyl acetate and hexanes. Yield = 3.6 g. ^{1}H NMR δ (ppm): 7.39 (m, $–C_6H_5$), 6.40 (s, –C(O)NHCH–), 5.14 (s, –OCH_2 (C_6H_5)), 4.88 (s, $–CH_2$$NH$C(O)–), 4.31 ($s$, –C(O)NH$CH$–), 3.24 ($t$, $–CH_2$NHC(O)–), 1.86 (d, –CH$CH_2$$CH_2CH_2$ CH_2NH–), 1.59 (d, $–CHCH_2$$CH_2$$CH_2CH_2$NH–), 1.45 ($s$, $–CHCH_2CH_2$$CH_2$$CH_2$NH–). Bis($N$-succinimido)-6,6-dithiobis(hexyl succinate), which was used as a cross-linker, was synthesized according to a previously reported procedure using thiohexanoic acid.[28] ^{1}H NMR δ (ppm): 4.10 (t, $–S(CH_2)_5$$CH_2$O–), 2.96 ($t$, $–SCH_2$$(CH_2)_5$O–), 2.82 ($s$, –NC(O)$CH_2$$CH_2$C(O)–), 2.71 ($t$, –C(O)$CH_2$$CH_2$C(O)ON–), 2.66 ($t$, –C(O)$CH_2$$CH_2$ C(O)ON–), 1.71–1.63 (t, $–SCH_2CH_2$$(CH_2)_2$$CH_2CH_2$–), 1.40 ($t$, $–SCH_2$$CH_2$$(CH_2)_2$$CH_2$$CH_2$–).

2.5. Preparation of NCPMs and CPMs

NCPMs were prepared using mPEG-PLA-Lys_4 polymeric micelles via the organic solvent/water emulsion method.[1] PEG-PLA-Lys_4 (50 mg) was dissolved in methylene chloride (2 mL), and the resulting polymer solution was added dropwise into distilled water (100 mL) under vigorous stirring in an open air system to evaporate methylene chloride. To prepare CPMs, bis(N-succinimido)-6,6-dithiobis (hexyl succinate) (2 wt% of polymer) was dissolved in methylene chloride (1 mL), and the resulting mixture was added dropwise into a solution of NCPMs (100 mL) under vigorous stirring. The cross-linking process proceeded until the organic solvent evaporated completely.

2.6. Stability of PMs and CPMs

The stability of NPMs and CPMs was estimated using sodium dodecyl sulfate (SDS) acting as a destabilizing agent. The effect of SDS on micelles was investigated via DLS. A solution of SDS solution (5 g/L, 1 mL) was added to the micelles solution (2 mL, 0.5 g/L), and the intensity of scattered light was monitored at predetermined time intervals.

2.7. SAXS Measurements

SAXS measurements were carried out using the 4C SAXS II beamline (BL) of the Pohang Light Source II (PLS II) at Pohang University of Science and Technology (POSTECH) at a power of 3 GeV. The light source from an In-vacuum Undulator 20 (IVU 20: length = 1.4 m, period = 20 mm) of the Pohang Light Source II storage ring was focused using a vertical focusing toroidal mirror coated with rhodium and monochromatized with a Si (111) double crystal monochromator (DCM), giving an X-ray beam with a wavelength of 1.216 Å. The X-ray beam size at the sample stage was 0.2 (V) × 0.6 (H) mm^2. A two-dimensional (2D) charge-coupled detector (Mar USA, Inc.) was employed, and a sample-to-detector distance (SDD) of 4.0 m and 0.5 m was used. The magnitude of scattering vectors $q = (4\pi/\lambda)\sin\theta$ was 0.05 nm^{-1} < q < 7.15 nm^{-1}, where 2θ is the scattering angle and λ is the wavelength of the X-ray beam source. The scattering angle was calibrated with polystyrene-b-polyethylene-b-polybutadiene-b-polystyrene (SEBS) block copolymer standards. Sample cells containing mica windows with a thickness of 10 μm, a volume of 50 μL, and an X-ray beam path length of 0.8 mm were used. All of the scattering measurements were carried out at 25 °C. The SAXS data were collected in 10 successive frames of 30 sec each to monitor radiation damage. The absence of changes in the scattering patterns over time indicated that radiation damage did not occur during the scattering measurements. Sample solutions with a concentration of 1 mg/mL were measured to obtain good quality scattering data without interference between micelles (i.e., to eliminate concentration effects). Each 2D SAXS pattern was circularly averaged from the beam center and normalized to the intensity of the transmitted X-ray beam (monitored with a scintillation counter located behind the sample cell). The scattering of the solvent (water) was used as the experimental background.

2.8. SAXS Models

For an isotropic two-phase system separated by sharp interfaces and consisting of polydisperse particles (phase 1) with scattering length b_1 and volume fraction ϕ_1 in a matrix (phase 2) of scattering length b_2 and volume fraction $\phi_2 = 1 - \phi_1$, the scattered intensity per unit volume can be expressed as follows:[29,30]

$$I(q) = (b_1 - b_2)^2 \rho_N (\langle F^2(q)\rangle + \langle F(q)\rangle^2 [\langle Z(q)\rangle - 1]) \quad (1)$$

where $F(q)$ is the scattering amplitude or the Fourier transform of the particle form, ρ_N is the number density of particles, and $Z(q)$ is the lattice factor describing the spatial distribution of the particles. The angular brackets $\langle \ldots \rangle$ denote the average with respect to the particle size distribution and spatial distribution of particles, which are assumed to be independent. This decoupling approximation allows one to factorize the scattering intensity into contributions from the form factor and structure factor of the particle. Generally, the form factor for core and shell particles is given as follows:[31]

$$P(q) = [b_c F_c(q, R_c) + b_s F_s(q, R_c, R_m)]^2 \quad (2)$$

where b_c and b_s are the contrast factors of the core and shell, respectively, R_c is the core radius, and R_m is the overall micelle radius. Under contrast matching conditions, either b_c or b_s is equal to zero, such that the form factors of the core and shell can be estimated independently. The functions for the shell, F_s (q, R_c, R_m), can be expressed in terms of the simpler function F (q, R):

$$F(q, R_c, R_m) = \frac{1}{1-p^{(3-\alpha)}} \times [F(q, R_m) - p^{(3-\alpha)} F(q, R_c)] \quad (3)$$

where $p = R_c/R_m$. The functions F (q, R) are fundamentally equal to the Fourier transform of the density profile $\phi(r)$. According to the Daoud-Cotton model, we consider hyperbolic density profiles of the general form $\phi(r) = r^{-\alpha}$, for which:

$$F(q, R) \equiv \frac{\int_0^R r^{-\alpha} \sin(qr) r^2/(qr)\, dr}{\int_0^R r^{-\alpha} r^2\, dr} = {}_1F_2\left(\frac{3-\alpha}{2}, \frac{3}{2}, \frac{5-\alpha}{2}; -\frac{q^2R^2}{4}\right) \quad (4)$$

where $\alpha \neq 3$ (${}_1F_2$ is the hypergeometric function). For a homogeneous layer, $\alpha = 0$, whereas dense d-dimensional polymer layers or brushes theories predict $\alpha = 2(d-1)/3$. Because polydispersity has remarkable effects on the scattering pattern, the form factor $P(q)$ was averaged over particle size distribution $h(R)$, for which we chose the Schulz-Zimm distribution, which is characterized by mean $\bar{R}$ and relative standard deviation σ_R. The model-dependent program SCATTER was used to obtain more detailed information on core/shell particle shape, size, and size distribution.[29–31]

3. RESULTS AND DISCUSSION

mPEG-PLA-Lys_4 was synthesized through the ring-opening polymerization of Lys(Z)-NCA with amine-functionalized mPEG-PLA as a macroinitiator and subsequent deprotection (Scheme 1). mPEG-PLA was reacted with Boc-6-Ahx-OH, and DCC was used to introduce an amine group at the end of the PLA block. The ^{1}H NMR spectrum of mPEG-PLA-Ahx-Boc is shown in Figure 1(a). A peak corresponding to the Boc group appeared at 1.38 ppm. Based on the integral ratio of the methyl peaks of the Boc at 1.38 ppm and those of the mPEG block at 3.40 ppm, the reaction was quantitative. The elimination of the Boc group was carried out with TFA. The disappearance of the peak at 1.38 ppm indicated the complete removal of the Boc group (Fig. 1(b)). The reaction of N^6-carbobenzyloxy-L-lysine with TCF in the presence of activated charcoal gave Lys(Z)-NCA in high yield. The ring-opening polymerization of Lys(Z)-NCA with mPEG-PDLLA-NH_2 as a macroinitiator was carried out in a mixture of $CHCl_3$ and DMF under nitrogen, and the product was isolated by precipitation from cold diethyl ether with high conversion. The ^{1}H NMR spectrum of mPEG-PLA-$Lys(Z)_4$ is shown in Figure 1(c). The peaks at 7.31 and 4.97 ppm were assigned to the protons of the benzyl group of the Lys(Z) block. The integral ratio of the benzene protons at 7.31 ppm to the methyl protons of the mPEG block at 3.40 ppm yielded the degree of polymerization (DP) of the Lys(Z) block. When the molar feed ratio of Lys(Z)-NCA to mPEG-PLA-NH_2 was 5, the DP of the Lys(Z) block was 4.2. The deprotection of the benzyl group of mPEG-PLA-$Lys(Z)_4$ was achieved by treatment with a mixture of TFA and HBr, as confirmed by the ^{1}H NMR spectrum (Fig. 1(d)). The disappearance of the peaks corresponding to the benzene ring at 7.31 ppm and the methylene protons adjacent to the benzene ring at 4.97 ppm indicated that the protective benzyl group of the polymer was completely removed. The broad peak at 7.71 ppm was assigned to the amine protons (–NH(CO)–) of amide groups.

CPMs were prepared by adding cross-linking agent to polymeric micelles formed by the organic solvent/water emulsion method. Cross-linking was confirmed by measuring the stability of micelles upon SDS addition, which acts as a destabilizing agent in aqueous media. The relative intensity obtained from DLS was normalized based on the scattering intensity of the first measurement of each solution. As shown in Figure 2, NCPMs exhibited an abrupt decrease in scattered light and the relative intensity was decreased to less than 70% within 1 h. In contrast, the relative intensity of CPMs remained greater than 90% after 6 h, indicating that the amine groups of NCPMs were reacted with the cross-linking agent to form highly stable CPMs.

The size of the polymeric micelles was obtained via DLS analysis. From the size distribution of the micelles shown in Figure 3 (a), the average diameter of NCPMs was 19.1 nm. Considering that the size of precursor polymer micelles (mPEG5K-PLA3K) was 26.8 nm, the size of NCPMs was significantly decreased, which could be due to the hydrophilic lysine units exposed in water. The zeta-potentials of polymeric micelles were measured in solution to verify the reason for the reduced size. It is noticeable that the zeta-potentials of precursor and mPEG-PLA-Lys_4 micelles are −9.75 and 12.20 mV, respectively, which is much higher than that of precursor polymer micelles. The increased zeta potential indicated that the exposed amine groups led to the change of surface charge and size. The zeta potential of CPMs after cross-linking was 0.89 mV, which was much lower than NCPMs. The decreased zeta potential reflects the conversion of primary amine groups of lysine units to amide linkages formed during cross-linking. The mean diameter of CPMs was increased to 29.2 nm through cross-linking process. Those results indicated that the chemical network structure formed in the core through the reaction of hydrophobic

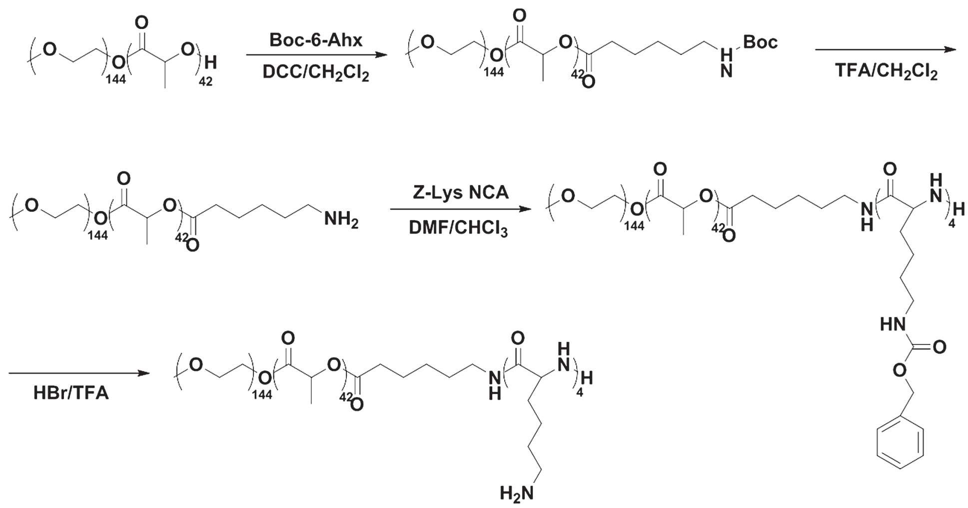

Scheme 1. Synthesis of mPEG-PLA-Lys$_4$.

cross-linking agents and amine groups. The TEM images also showed that the size of the micelles increased after cross-linking (Figs. 3(c) and (d)). The polymeric micelles were spherical in shape, and their sizes were in close agreement with those obtained from DLS. Thus, aggregation between micelles did not take place during the cross-linking process.

Figure 4 shows the SAXS curves of NCPMs and CPMs in aqueous solution at 25 °C. These SAXS curves were quantitatively analyzed using the form factor of the core/shell nanoparticle model with a Schulz-Zimm distribution, based on the assumption that core/shell micelle molecules are spherical and have a homogeneous core and shell layer with sharp interfaces.[31] The SAXS curves obtained by fitting data obtained from SCATTER software were in good agreement with the experimental data in the entire q range. The structural parameters obtained from the analysis of the SAXS curves are listed in Table I. The cross-linking agent incorporated into the polymer micelles chemically reacted with the amine groups, which increased the overall micelle radius from 11.90 nm to 13.70 nm. The average core radius of CPMs was 1.460 nm, while that of NCPMs was 3.220 nm. The observed reduction in the core radius was due to the formation of a more densely packed structure, which was attributed to cross-linking, as shown by a decrease in the *Rho* value (ratio of the shell to core density) of CPMs.

The particle size distribution of the core and overall micelle of NCPMs and CPMs was obtained using R_c, R_m, and the corresponding σ_R values (Fig. 5). As shown in Figure 5(a), the core of NCPMs exhibited a slightly

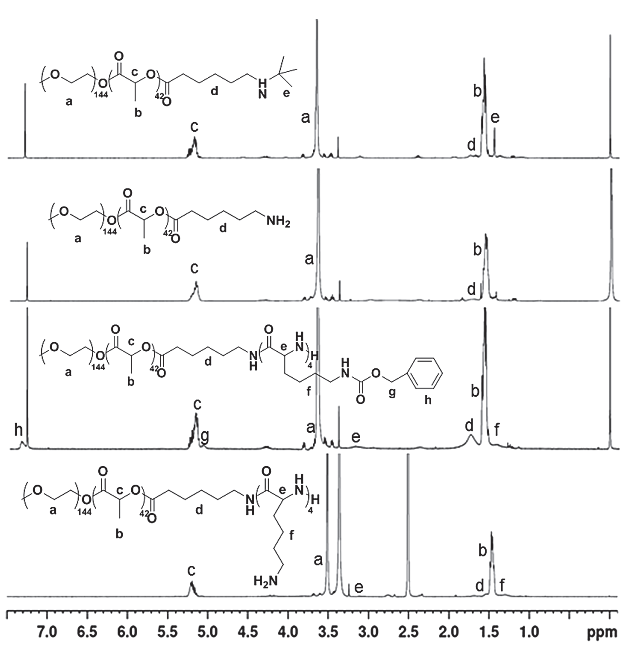

Figure 1. The ^{1}H NMR spectra of (a) mPEG-PLA-Ahx-Boc, (b) mPEG-PLA-NH$_2$, (c) mPEG-PLA-Lys(Z) in CDCl$_3$, and (d) mPEG-PLA-Lys$_4$ in DMSO.

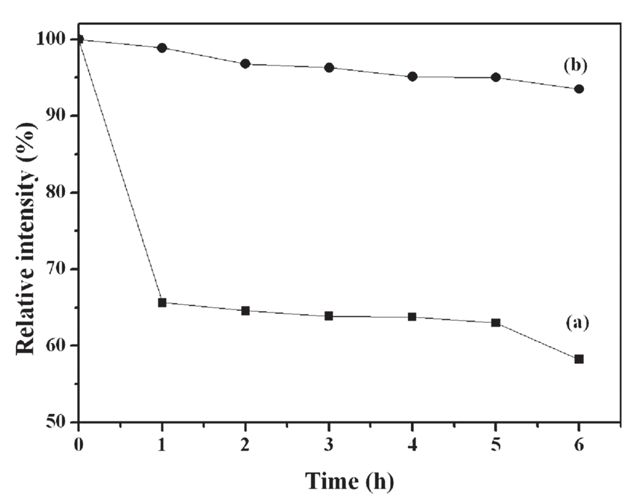

Figure 2. Stability of (a) NCPMs and (b) CPMs over time upon SDS addition.

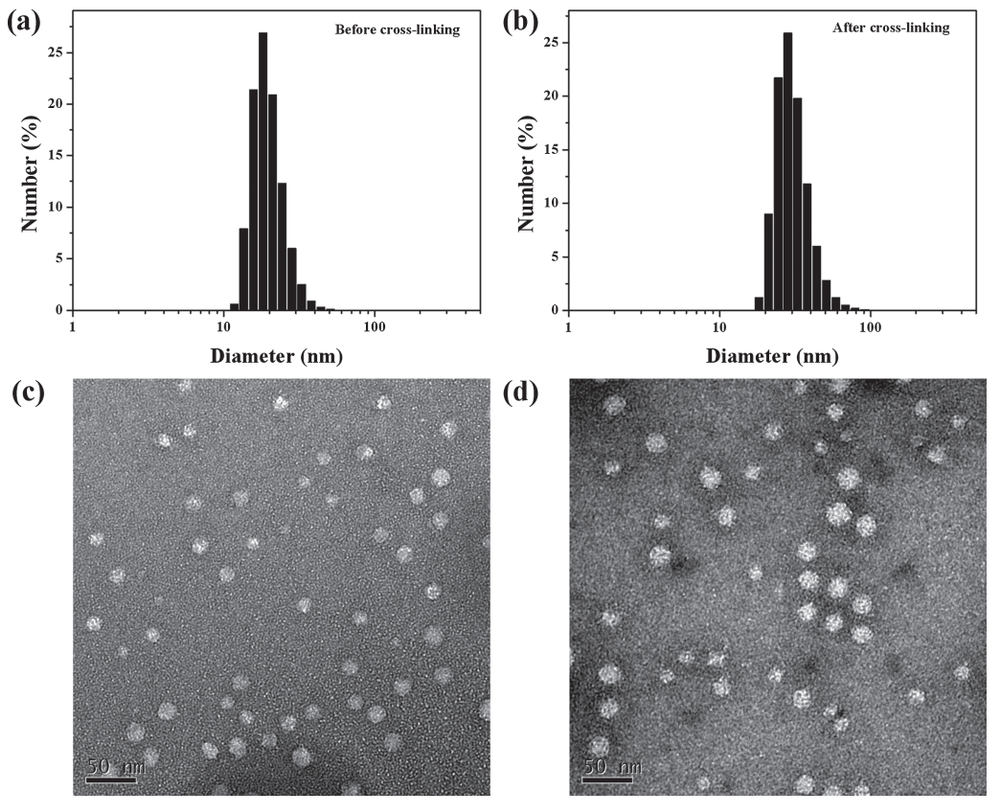

Figure 3. The size distribution of (a) NCPMs and (b) CPMs measured via DLS, and TEM images of (c) NCPMs and (d) CPMs.

broader size distribution (FWHM = 2.47 nm) than that of CPMs (FWHM = 1.11 nm), which was attributed to the natural self-assembly of the core due to attractive interactions among hydrophobic terminal groups in the center of NCPM. The $h(R)$ of CPM displayed a relatively narrow pattern, because the core originated from chemically well-defined cross-linking agent molecules incorporated into the micelles. As shown in Figure 5(b), for the overall micelle, the $h(R)$ for CPMs (FWHM = 10.39 nm) was approximately the same as that of NCPMs (FWHM = 9.11 nm). These results were consistent with those of the TEM and DLS analysis, even though variations in the average overall

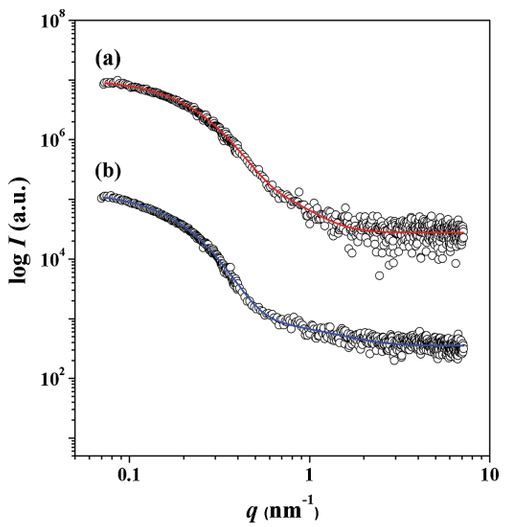

Figure 4. Scattering profiles of (a) NCPMs and (b) CPMs. The symbols represent the experimental data, and the solid lines are the fitted data, which were obtained using SCATTER. Each plot is shifted along the log I axis for clarity.

Table I. Summary of the structural parameters obtained from SAXS measurements of NCPM and CPM.

Sample	NCPMs		CPMs	
Model	Sphere		Sphere	
Type	Homogeneous core and shell		Homogeneous core and shell	
[a] R_c (nm)	3.220	[b](4.317)	1.460	[b](1.914)
[c] σ_R	0.326	–	0.322	–
[d] $R_{c,\max}$ (nm)	2.888	[e](3.944)	1.228	[e](1.732)
[f] R_m (nm)	11.90	[g](15.69)	13.70	[g](17.96)
[h] $R_{m,\max}$ (nm)	10.61	[i](14.48)	12.21	[i](16.40)
[j] *Rho*	0.106	–	0.019	–

Notes: [a]Average core radius estimated from the particle size distribution; [b]Average core radius estimated from the particle volume distribution; [c]Relative standard deviation (RSD = standard deviation/mean value) of R_c; [d]Core radius at the maximum particle size distribution; [e]Core radius at the maximum particle volume distribution; [f]Average overall micelle radius estimated from the particle size distribution; [g]Average overall micelle radius estimated from the particle volume distribution; [h]Overall micelle radius at the maximum particle size distribution; [i]Overall micelle radius at the maximum particle volume distribution; [j]Ratio of the shell and core density at the interface ($Rho = \phi_{CS}/\phi_C$).

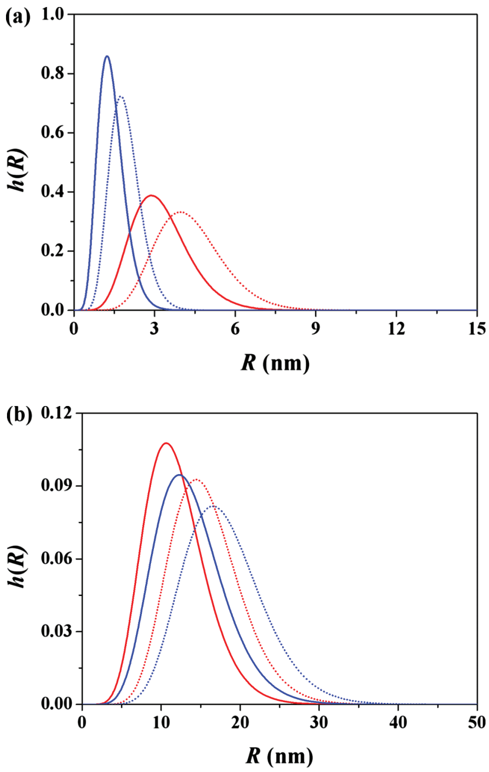

Figure 5. Particle size and distribution of (a) NCPMs and (b) CPMs, based on the analysis of experimental SAXS data using SCATTER software. The red and blue lines are the distribution of NCPMs and CPMs, respectively. The solid and dotted lines are the particle size and volume distribution, respectively.

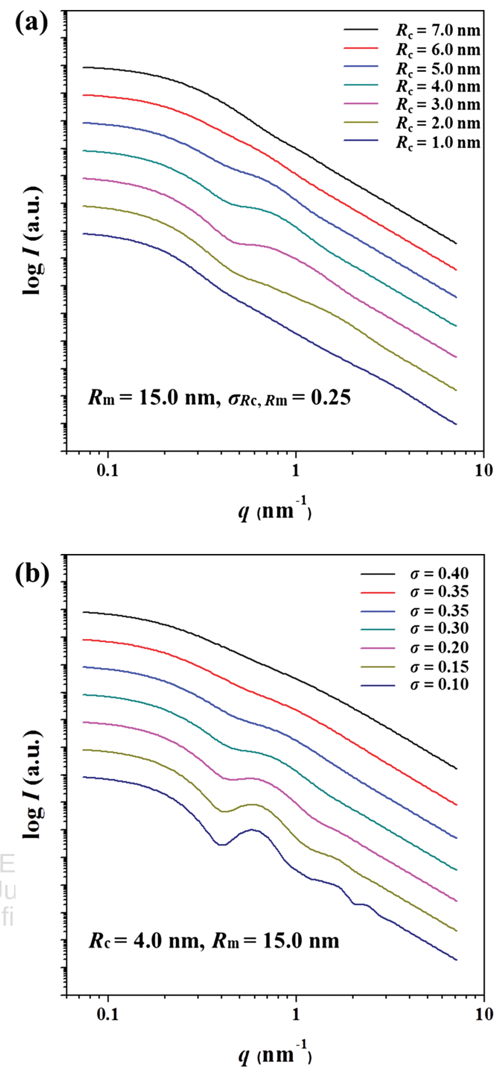

Figure 6. Change of theoretical SAXS curves of the core/shell polymeric micelles in response of change in (a) core radius R_c and (b) its relative standard deviation σ value.

micelle radii were observed. The particle volume distribution, which was calculated by determining the relationship between the number of particles of the same size and the volume of those particles, shifted toward the long distance R region compared to the particle size distribution. For the better understanding of the changes of X-ray scattering patterns in response to variations in structural parameters, such as R_c, R_m, and their σ values, we attempted to calculate the theoretical SAXS curves of the core/shell polymeric micelle over the whole q range. Figure 6(a) clearly shows the changes of the theoretical SAXS curves of the core/shell polymeric micelle in response to changes in the core radius R_c under the assumption that $R_m = 15.0$ nm, σ_{R_c} $(= \sigma_{R_m}) = 0.25$. As seen in Figure 6(a), as the core radius R_c was increased from 1.0 nm to 7.0 nm, the scattering patterns corresponding to the core part in a q range between 0.4 nm^{-1} and 1.1 nm^{-1} disappeared in a stepwise manner, with its scattering pattern shifted toward small q region. Figure 6(b) clearly shows the changes of the theoretical SAXS curves of the core/shell polymeric micelle in response to changes in the σ values of both the core radius R_c and the overall micelle radius R_m, based on the assumption that $R_c = 4.0$ nm, $R_m = 15.0$ nm. As seen in Figure 6(b), as the σ_{R_c} $(= \sigma_{R_m})$ value of the core radius R_c and the overall micelle radius R_m was increased from 0.10 to 0.40, the high order oscillation scattering patterns in a q range between 0.4 nm^{-1} and 3.0 nm^{-1} disappeared gradually, at the same time its scattering pattern smeared out.

4. CONCLUSIONS

We synthesized mPEG-PLA-Lys_4 as a reactive amphiphilic polymer and investigated the structural changes of polymeric micelles due to cross-linking. The polymeric micelles were cross-linked by reacting lysine amino groups with a hydrophobic cross-linking agent, which was incorporated into the micelles, and an increase in the overall micelle radius and a decrease in the core radius were observed. Investigations of the *in vitro* drug release of CPMs in response to a reducing agent such as glutathione are now underway.

Acknowledgments: This work was supported by the DGIST R&D Program (13-NB-01 and 14-NB-02) of the

Ministry of Education, Science, and Technology of Korea (MEST). Synchrotron X-ray scattering measurements performed at the Pohang Accelerator Laboratory were supported by MEST (Basic Science Research Project No. 20090072614).

References and Notes

1. K. Kataoka, A. Harada, and Y. Nagasaki, *Adv. Drug Deliv. Rev.* 47, 113 (**2001**).
2. S. Ganta, H. Devalapally, A. Shahiwala, and M. Amiji, *J. Control. Release* 126, 187 (**2008**).
3. S. Stolnik, L. Illum, and S. S. Davis, *Adv. Drug Deliv. Rev.* 16, 195 (**1995**).
4. G. S. Kwon, *Crit. Rev. Ther. Drug Carrier Syst.* 15, 481 (**1998**).
5. R. Savic, T. Azzam, A. Eisenberg, and D. Maysinger, *Langumir* 22, 3570 (**2006**).
6. H. Chen, S. Kim, W. He, H. Wang, P. S. Low, and K. Park, *Langumir* 24, 5213 (**2008**).
7. K. Letchford and H. M Burt, *Mol. Pharm.* 9, 248 (**2012**).
8. M. Iijima, Y. Nagasaki, T. Okada, M. Kato, and K. Kataoka, *Macromolecules* 32, 1140 (**1999**).
9. L. Zhang, K. Katapodi, T. P. Davies, C. Barner-Kowollik, and M. H. Stenzel, *J. Polym. Sci. A Polym. Chem.* 44, 2177 (**2006**).
10. T. K. Bronich, P. A. Keifer, L. S. Shlyakhtenko, and A. V. Kabanov, *J. Am. Chem. Soc.* 127, 8236 (**2005**).
11. J. A. Zupancich, F. S. Bates, and M. A. Hillymer, *Biomacromolecules* 10, 1554 (**2009**).
12. P. Bhargava, J. X. Zheng, P. Li, R. P. Quirk, F. W. Harris, and S. D. Cheng, *Macromolecules* 39, 4880 (**2006**).
13. T. Riley, T. Govender, S. Stolnik, C. D. Xiong, M. C. Garnett, L. Illum, and S. S. Davis, *Colloids Surf. B: Biointerfaces* 16, 147 (**1999**).
14. T. Riley, S. Stolnik, C. R. Heald, C. D. Xiong, M. C. Garnett, L. Illum, S. S. Davis, S. C. Purkiss, R. J. Barlow, and P. R. Gellert, *Langmuir* 17, 3168 (**2001**).
15. S. A. Hagan, S. S. Davis, L. Illum, M. C. Davies, M. C. Garnett, D. C. Taylor, M. P. Irving, and T. F. Tadros, *Langmuir* 11, 1482 (**1995**).
16. O. Glatter, G. Scherf, K. Shillen, and W. Brown, *Macromolecules* 27, 6046 (**1994**).
17. D. I. Vergun, *J. Appl. Crystallogr.* 33, 530 (**2000**).
18. L. A. Feigin and D. I. Svergun, Structure Analysis by Small-Angle X-ray and Neutron Scattering, Plenum Press, New York (**1987**).
19. R. J. Roe, Methods of X-ray and Neutron Scattering in Polymer Science, Oxford University Press, New York (**2000**).
20. P. Hickel, M. Ballauff, and A. Jada, *Macromolecules* 29, 4006 (**1996**).
21. C. Dupty, X. Auvray, C. Petipas, and R. Anthore, *Langmuir* 12, 3162 (**1996**).
22. T. Riley, C. R. Heald, S. Stolnik, M. C. Garnett, L. Illum, S. S. Davis, S. M. King, R. K. Heenan, S. C. Purkiss, R. J. Barlow, P. R. Gellert, and C. Washington, *Langmuir* 19, 8428 (**2003**).
23. M. Nakano, M. Deguchi, K. Matsumoto, H. Matsuoka, and H. Yamaoka, *Macromolecules* 32, 7437 (**1999**).
24. L. He, V. M. Garamus, S. S. Funari, M. Malfois, R. Willumeit, and B. Niemeyer, *J. Phys. Chem. B* 106, 7696 (**2002**).
25. J. S. Pedersen, C. Svaneborg, K. Almdal, I. W. Hamley, and R. N. Young, *Macromolecules* 36, 416 (**2003**).
26. J. Bhattacharjee, G. Verma, V. K. Aswal, and P. A. Hassan, *Pramana* 71, 991 (**2008**).
27. A. Isamu, T. Naotaka, H. Satoshi, and S. Kazuo, *Langmuir* 26, 7544 (**2010**).
28. S.-K. Lee, H.-C. Kim, S.-J. Cho, S. W. Jeong, and W. B. Jeon, *Ultramicroscopy* 108, 1374 (**2008**).
29. S. Förster, A. Timmann, M. Konrad, C. Schellbach, A. Meyer, S. S. Funari, P. Mulvaney, and R. Knott, *J. Phys. Chem. B* 109, 1347 (**2005**).
30. S. Förster, E. Wenz, and P. Lindner, *Phys. Rev. Lett.* 77, 95 (**1996**).
31. S. Förster, A. Timmann, C. Schellbach, A. Frömsdorf, A. Kornowski, H. Weller, S. V. Roth, and P. Lindner, *Nat. Mater.* 6, 888 (**2007**).

Received: 16 October 2014. Accepted: 28 March 2015.